Cathodoluminescence defect characterization of hydrothermally grown Sn O 2 nanoparticles

U. Pal, A. Pérez-Centeno, and M. Herrera-Zaldívar

Citation: Journal of Applied Physics **103**, 064301 (2008); doi: 10.1063/1.2885060
View online: http://dx.doi.org/10.1063/1.2885060
View Table of Contents: http://scitation.aip.org/content/aip/journal/jap/103/6?ver=pdfcov
Published by the AIP Publishing

Cathodoluminescence defect characterization of hydrothermally grown SnO_2 nanoparticles

U. Pal,[1,a)] A. Pérez-Centeno,[1] and M. Herrera-Zaldívar[2]
[1]*Instituto de Física, Universidad Autónoma de Puebla, Apdo. Postal J-48, Puebla, Puebla 72570, Mexico*
[2]*Centro de Ciencias de la Materia Condensada, Universidad Nacional Autónoma de Mexico, Apdo. Postal 2681, Ensenada, B.C., 22800 Mexico*

(Received 23 November 2007; accepted 20 December 2007; published online 17 March 2008)

SnO_2 nanoparticles in the 50–150 nm size range were grown by a low temperature hydrothermal process, using $SnCl_4 \cdot 5H_2O$ as precursor and $CH_3(CH_2)_{15}N(Br)(CH_3)_3$ as stabilizing agent. The as-grown samples were mostly amorphous and their crystallinity improved either by prolonged hydrothermal process or by air annealing at high temperatures. The absence of near-band-edge emission and appearance of a broad visible emission related mainly to oxygen vacancies and crystalline defects were the main characteristics of their room temperature cathodoluminescence (CL) spectra. A luminescent band in the 1.79–1.83 eV spectral region was also detected. The intensity of the defect bands reduces both on prolonged hydrothermal treatment and air annealing at high temperatures, indicating a net decrease of defect content on thermal treatments. Panchromatic CL images revealed that most of the defect emissions come from smaller SnO_2 nanoparticles.
 [DOI: 10.1063/1.2885060]

I. INTRODUCTION

Semiconducting metal oxide nanostructures have interesting optical, electrical, and chemical properties to be used for a range of applications.[1] In particular, tin dioxide (SnO_2) is a *n*-type semiconductor with wide band gap (E_g=3.7 eV at 300 °C) (Ref. 2) with applications in catalysis,[3] gas sensing,[4,5] transparent conducting electrodes,[6] and transistor.[7] An intriguing catalytic application of metal oxides is the surface deactivation of organophosphorus-based chemical warfare agents.[3] High surface areas of small SnO_2 nanoparticles have been reported to increase the efficiency of anode in Li-secondary battery.[8]

SnO_2 can be synthesized by several growth methods, for example, thermal evaporation of oxide powder,[9] hydrothermal synthesis,[10,11] rapid oxidation of the tin,[12] combustion chemical vapor deposition,[13] spray pyrolysis,[14] and chemical solution routes.[15] Recent trend of synthesizing SnO_2 nanostructures is based on the control of their size, shape, and defect distribution by cheap and easy process. Hydrothermal synthesis is an adequate method to prepare SnO_2 nanostructures with good control of size. However, there are few reports on SnO_2 synthesis by hydrothermal process.

In this work, we present the preparation of SnO_2 nanopowders by a low temperature hydrothermal process and their cathodoluminescence (CL) properties. Apart from CL, the nanostructures were also characterized by scanning electron microscopy (SEM), x-ray diffraction (XRD), energy dispersive spectroscopy (EDS), and Fourier-transform infrared (FTIR) spectroscopy techniques in order to evaluate their morphology, crystalline, and optical properties.

[a)]Author to whom correspondence should be addressed. Electronic mail: upal@sirio.ifuap.buap.mx. FAX: +52-222-2295611.

II. EXPERIMENTAL DETAILS

The SnO_2 nanopowders were grown by hydrothermal method at 120 °C, using $SnCl_4$ as precursor. We dissolved 3 g of $SnCl_4 \cdot 5H_2O$, 2 g of $CH_3(CH_2)_{15}N(Br)(CH_3)_3$ (CTAB), and 1.711 g of NaOH into 80 ml de-ionized water in a three necked round bottom flask. In this step, the mixture had a whitish color. The mixture was stirred for 10 min at room temperature (RT) and then heated to 120 °C. This temperature was maintained either for 16 h (sample A) or for 48 h (sample B). After cooling down, the samples were washed with de-ionized water once and ethanol twice under centrifuge at 15 000 rpm for 10 min. Then, the samples were dried at RT. In order to improve the crystalline quality, both samples were annealed for 2 h at 300 °C (renamed as samples A1 and B1) or 550 °C (renamed as samples A2 and B2). The morphology and chemical composition of the SnO_2 powders were evaluated by a SEM (JEOL JSM-5300) with Noran analytical system attached. The CL system attached to this SEM includes a SPEX 340E monochromator and a Keithley 427 current amplifier. For CL studies, electron beam of 25 keV and a filament current of 27 nA were used. A Hamamatsu R928P photomultiplier was used for recording the CL spectra and panchromatic images of the samples. The monochromator was manipulated from a personal computer and the acquired CL spectra were corrected for the monochromator and detector responses. The crystallinity of the samples was examined by Phillips X'pert x-ray diffractometer with a (λ=0.154 nm) CuKα line as excitation source. The FTIR studies were carried out by a Nicolet Magna 750 FTIR spectrometer. All the measurements were performed at RT.

III. RESULTS AND DISCUSSION

Typical SEM images of the as-grown SnO_2 powders can be seen in the Figs. 1(a) and 1(b) for the samples A and B,

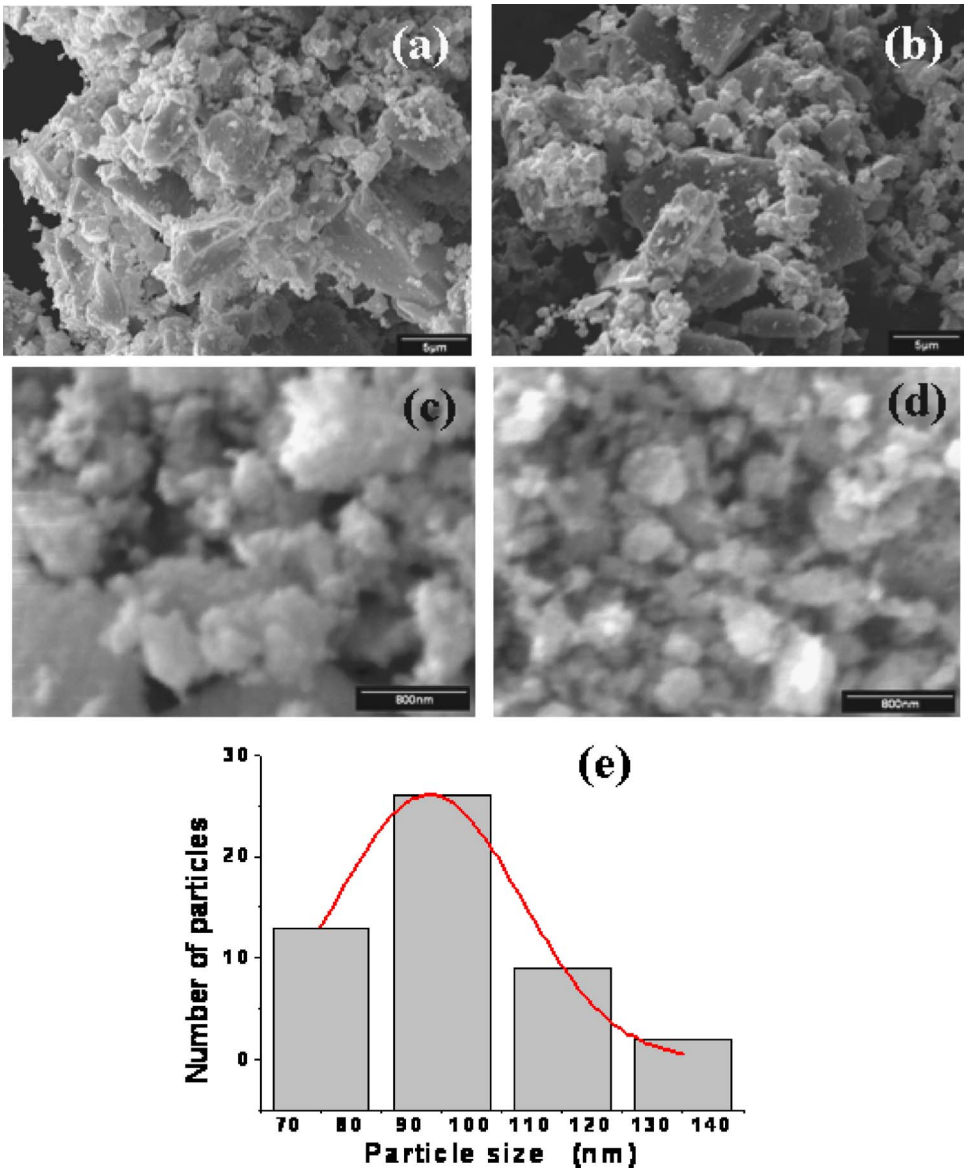

FIG. 1. (Color online) Typical SEM images of the SnO_2 nanopowders prepared for (a) 16 h and (b) 48 h of hydrothermal treatments at 120 °C (samples A and B, respectively). Typical SEM images of (c) sample A after annealing for 2 h at 550 °C (renamed as sample A2) and (d) sample B after annealing for 2 h at 550 °C (renamed as sample B2), with (e) its particle size distribution histogram.

respectively. Formation of inhomogeneous SnO_2 particles can be seen from the images. Inspecting both images with more details, we can identify the presence of SnO_2 particles of nanometer size. However, bigger particles of the order of few microns formed by agglomeration of smaller particles are observed too. Therefore, the SnO_2 samples are not completely broken until this step. Typical SEM images of samples A and B after annealing at 550 °C for 2 h are presented in the Figs. 1(c) and 1(d), respectively. The SEM images of the annealed samples [Figs. 1(c) and 1(d)] present SnO_2 nanopowders with more homogenous sizes but still, there remain bigger SnO_2 agglomerates. A quarter of the Fig. 1(d) was processed to measure the size of the SnO_2 particles and its size distribution is illustrated in the Fig. 1(e). The average particle size of the sample was estimated to be about 94 nm from the Gaussian fit to the size distribution histogram. Similar processes were applied to the other annealed samples. The average particle size of the SnO_2 nanopowders varied in between 90 and 130 nm.

The XRD patterns for the four annealed samples are graphed in the Fig. 2. Figures 2(a)–2(d) correspond to the samples A1, A2, B1, and B2, respectively. It must be mentioned that the XRD patterns of the as-grown samples did not reveal any diffraction peak, indicating their amorphous nature. There appeared distinct diffraction peaks in the annealed samples corresponding to tetragonal rutile phase of SnO_2 with lattice constants $a=0.4738$ nm and $c=0.3187$ nm. Miller indices of each diffraction peak are indicated in Fig. 2 and the interplaner spacings agreed well with the standard data file.[16] From the Figs. 2(a) and 2(b), we can note that the diffraction intensity increased and the full width at half maximum (FWHM) decreased on increasing the annealing temperature for the sample prepared for 16 h of growth time. Similar trend can be observed from the Figs. 2(c) and 2(d) for the SnO_2 powders prepared for 48 h of growth time. Therefore, thermal annealing process helps to crystallize the SnO_2 powders, perhaps, by removing oxygen vacancies and other crystal defects as we will see later. Now, if we observe only Figs. 2(a) and 2(c), we can distinguish that for 300 °C annealing temperature, SnO_2 has better crystalline quality when the growth time or hydrothermal treatment is longer. One more time, the same result can be de-

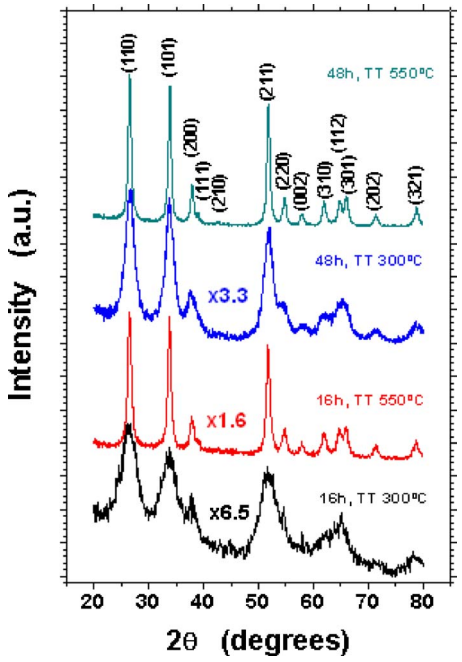

FIG. 2. (Color online) XRD patterns of the SnO_2 nanopowders after air annealing at different temperatures. Improvement of crystallinity in the samples by annealing at higher temperature is evident.

duced for annealing at 550 °C from the Figs. 2(b) and 2(c). Thus, the sample prepared for 48 h of growth time and post-growth air annealing at 550 °C [Fig. 2(d)] has best crystalline quality.

The crystallite size (d) for the annealed samples was estimated from their XRD patterns using the Scherrer equation: $d=0.9\lambda/B\cos\theta$; where λ is the wavelength of the irradiation, B is the FWHM of the diffraction peak in radian, and θ is the diffraction peak position. The estimated sizes of the crystalline nanograins were 27, 108, 47, and 115 nm for samples A1, A2, B1, and B2, respectively. Here, we must emphasize that the Scherrer equation calculates the average size of the crystalline domains, which means the crystalline grain size; whereas, from SEM images, we measure the size of the agglomerated nanocrystals. However, the betterment of crystallinity with prolonged hydrothermal treatment and air annealing at higher temperatures is very clear form the above results. Remembering the SEM results, we can note that for the samples annealed at 550 °C, the particle sizes calculated from both techniques are very similar. Therefore, we believe that the nanoparticles seen by SEM in the samples after annealing at 550 °C are almost monocrystalline.

CL is a powerful and efficient technique for the defect characterization in semiconductors and semiconductor nanostructures, especially for detecting their spatial distributions. However, very few CL studies have been reported on nanostructured SnO_2.

RT CL spectra of the samples A1 and B1 are presented in Fig. 3. There appeared a broad emission band in the 3.5–1.5 eV energy range for both samples, indicating multiple defect related emissions in them. However, the intensity of the CL emission is lower for sample B1, prepared with longer hydrothermal treatment. The CL spectra of sample

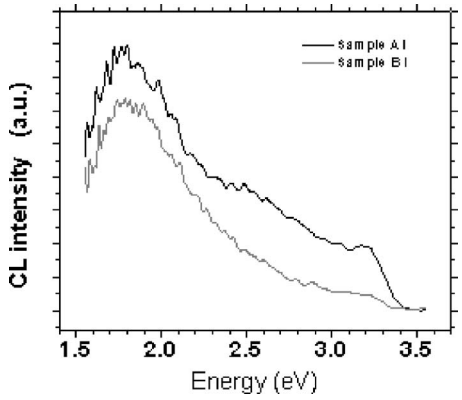

FIG. 3. Typical RT CL spectra of samples A1 and B1.

A2, annealed at 550 °C, are presented in Fig. 4. The integrated CL intensity of the samples reduced about 30% after annealing at 550 °C, indicating a reduction in defect density on annealing at higher temperature. On the other hand, the CL spectra of both the samples (A2 and B2) were quite similar.

Computer deconvolution of the broad CL band of sample A2 revealed three component bands centered around 1.85, 2.52, and 3.18 eV. We named those component bands as P1, P2, and P3, respectively. Similar deconvolution operations were carried out for the CL bands of the other samples. In Table I, the position and intensity of the component bands for all the samples are listed. From the table, we can see that P2 and P1 peak positions vary in opposite manner on thermal annealing. While the P2 peak suffers a redshift after annealing at 550 °C, P1 peak suffers a blueshift. The position of P3 peak remains almost at the same position after thermal treatment at 550 °C.

An emission band in the 390–400 nm (3.1–3.17 eV) region, similar to our P3 band, has been reported by several authors in their photoluminescence (PL) or CL spectra of SnO_2 nanostructures. The emission was assigned to surface dangling bonds[17,18] or to the oxygen vacancies and tin interstitials[17–20] in the nanostructured SnO_2. Exact origin of this band is yet unclear. A band in between 455 and 490 nm (2.5–2.7 eV), similar to our P2 band, has been assigned as the blue-green emission in SnO_2 nanostructures.[12,21,22] The origin of this emission band was assigned either to the structural defects during the growth of nanostructures[12,21] or oxygen vacancies.[22] Reduction of emission intensity of this band, either by prolonged hydrothermal treatment of air annealing at high temperature (Table I), justifies the above arguments.

On the other hand, to the best of our knowledge, it is the first time that SnO_2 nanoparticles revealed a luminescence emission band (P1 peak) in the 1.78–1.83 eV range at RT. Emission bands at about 620 nm (2 eV) and 640 nm (1.93 eV) have been reported by He *et al.*[23] and Kim *et al.*[24] in their PL spectra of one dimensional SnO_2 nanostructures and subsequently attributed to growth induced crystalline defects such as oxygen vacancies or tin interstitial. However, Maestre *et al.*[25] have reported a CL emission band at about 650 nm (1.9 eV) in the low temperature (80 K) CL spectra of SnO_2 nanostructures prepared by sintering commercial

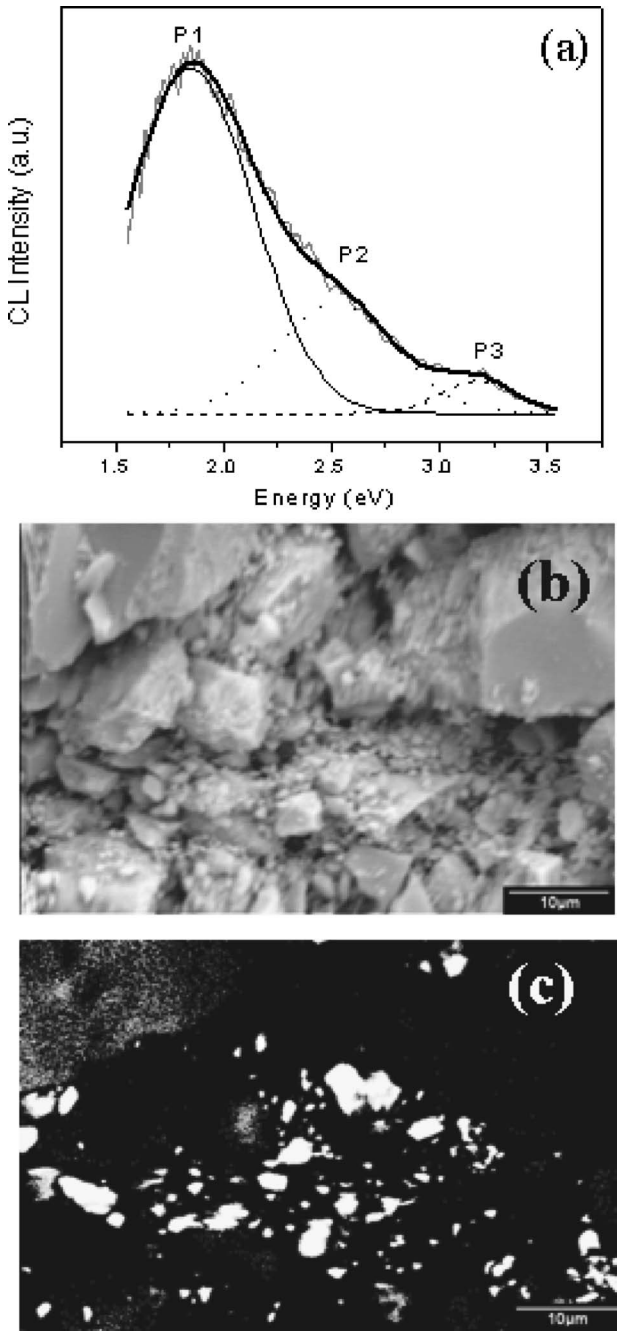

FIG. 4. (a) Typical RT CL spectrum, (b) secondary electron image, and (c) panchromatic CL image [of the area shown in (b)] of sample B2. The smaller SnO_2 particles emit higher intensity CL.

SnO_2 powders. They attributed the emission to both oxygen vacancy and structural defects. A complex intensity evolution of this band on thermal treatment and ball milling times leads them to predict a competition between creation and recovery of defects.

An emission band peaked in between 1.95 and 2.0 eV has been reported in the PL and CL studies of tin oxide. Cheng and Park[26] reported an orange PL band and suggested to be related to nonstoichiometry and other defects. Themlin *et al.*[27] have found that the defect states of most stable SnO_2(110) surface correspond to donor defect states at about 1.4 eV above the top of the valence band, which is compatible to the transitions leading to orange emission. A broad CL emission extending from green to orange spectral regions has been reported by Crabtree[28,29] and oxygen vacancies are suggested to be responsible.

TABLE I. A summary of the peak position and CL intensity of the component defect bands for all the samples.

	Peak position (eV)			CL intensity (a.u.)		
Sample	P1	P2	P3	P1	P2	P3
A1	1.78	2.73	3.19	44.39	14.58	5.07
A2	1.82	2.52	3.18	30.71	5.23	1.49
B1	1.80	2.58	3.12	31.51	2.66	1.29
B2	1.83	2.53	3.10	31.35	4.26	0.95

The position of the P1 band we observed in the orange spectral region varied from 1.84 to 1.78 eV (675–695 nm). By monitoring the position and intensity of the emission band, we can see (Table I) that both of them varied notably on variation of hydrothermal treatment time but did not vary much with increase of air annealing temperature. Such evolutions of the emission band suggest that the band is more regulated by the crystalline defects rather than electronic defects such as oxygen vacancies, for the used annealing temperature range.

From Table I, we can see that the P2 and P1 peak positions vary in opposite manner on air annealing. While P2 peak suffers redshifts after annealing, P1 peak suffers a blueshift. On the other hand, P3 peak does not change its position notably before and after annealing treatment. So, the emissions could be associated to different types of radiative recombination processes. However, the intensity of all the emissions reduces after thermal annealing process. Therefore, if the luminescence is associated with crystal defects, then, the annealing process helps to recrystallize the SnO_2 particles by removing the crystal defects in agreement with our XRD results.

It must be noted that we could not detect the near-band-edge (NBE) emission in our SnO_2 nanoparticles. Since in the CL process, the excitation occurs through highly energetic electrons, the absence of NBE emission in CL spectra indicates the real effect of high surface-to-volume ratio in the nanostructures. As a free semiconductor surface can present singly occupied atomic orbitals (dangling bonds) that can form two dimensional surface bands which may partly lie in the forbidden gap, it can result in a pinning of the Fermi level and of acceptor-like surface states in *n*-type samples as well as in the presence of a space charge layer.[30] The thickness of that depletion layer could be about 150 nm for SnO_2.[17] Therefore, the absence of NBE in our samples is justified due to their smaller average sizes and high surface-to-volume ratios.

Figures 4(b) and 4(c) are the secondary and panchromatic CL images, respectively, of the same area of sample B2. The images evidently suggest that the radiative recombinations come mainly from the smaller SnO_2 nanoparticles. In fact, the SnO_2 agglomerates or bigger particles do not emit. It is known that SnO_2 is not a good luminescent material in bulk form. The luminescence increases notably when in nanoparticle form.[31] Many good properties of SnO_2 are

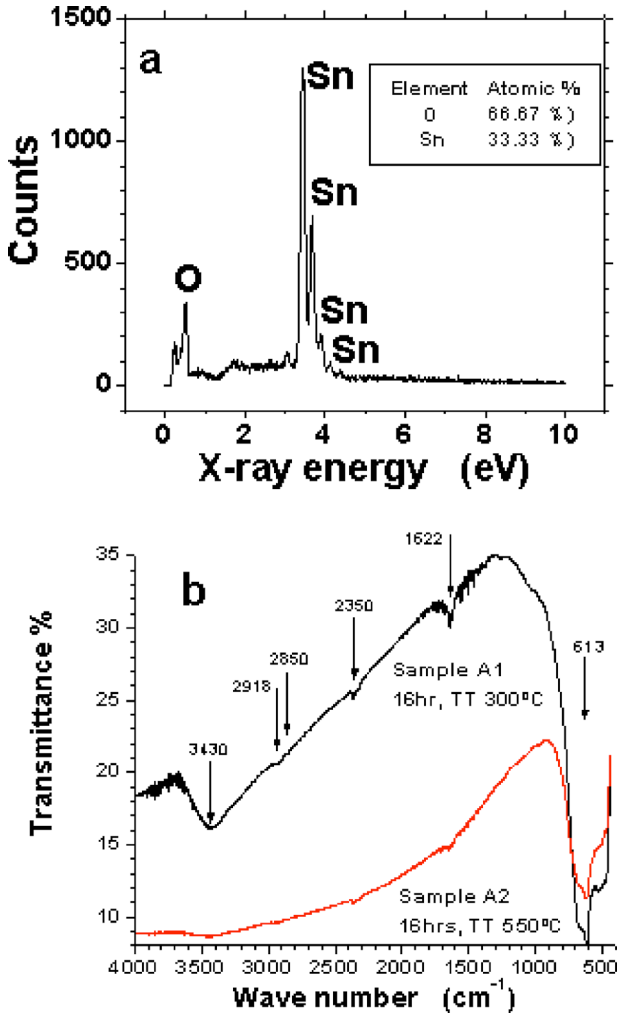

FIG. 5. (Color online) (a) Typical EDS spectrum of sample A2 and (b) FTIR transmittance spectra for samples A1 and A2.

related to impurities of crystal defect in the surface or interface, for example, the oxygen vacancies. The surface-to-volume ratio increases as SnO_2 goes to nanosize. So, maybe the defects attributed to the luminescence are more effective in nanoparticles than microparticles or in bulk.

Figure 5(a) shows a typical EDS spectrum and chemical composition for sample A2. The presence of only oxygen and tin was identified. Quantitative elemental analysis revealed about 66.67 and 33.33 at. % of O and Sn in the sample, which correspond to perfect stoichiometry of SnO_2. Same EDS results were obtained for the others sample after annealing.

The FTIR spectra for samples A1 and A2 are presented in Fig. 5(b). The transmittance spectra revealed four characteristic signals related to water, CTAB, CO_2, and SnO_2. The bands at 3430 and 1622 cm^{-1} are associated with water absorbed on the surface.[32,33] The band at 2350 cm^{-1} corresponds to the CO_2 traces in the atmosphere.[32,33] The bands at 2918 and 2850 cm^{-1} are related to the antisymmetric and symmetric vibrations of $C-CH_2$ bond of the CTAB.[34] The band at 613 cm^{-1} corresponds to the antisymmetric Sn–O–Sn mode of the tin oxide.[35,36] From the Fig. 4(b), we can determine that the washing process was not enough to remove completely the surfactant CTAB form the samples. On the other hand, the intensity of both signals related to water and CTAB reduces in sample A2. It means that annealing for 2 h at 550 °C is not enough to remove water trace. Finally, in both samples, SnO_2 related band (at about 613 cm^{-1}) is present. The intensity of this band increases after annealing at higher temperature. Thus, once again, it is evident that SnO_2 recrystallize by annealing at high temperature.

IV. CONCLUSIONS

SnO_2 nanoparticles of 50–150 nm size range could be prepared by low temperature hydrothermal process using $SnCl_4 \cdot 5H_2O$ as precursor and CTAB as surfactant. The crystallinity of the nanoparticles can be improved either by prolonged hydrothermal treatment or by thermal annealing at high temperatures in air ambient. The density of crystalline and oxygen vacancy related defects in the nanoparticles can be reduced by air annealing at high temperatures. The relative intensities of the defect bands depend on the time of hydrothermal treatment and postgrowth annealing temperature. While the blue-green defect band at around 2.52 eV is mainly related to defects during growth, the orange emission at about 1.82 eV is related to the oxygen vacancies and tin interstitials in SnO_2 nanoparticles. Stronger CL emissions from the smaller particles indicate the surface origin of the defect structures in SnO_2 nanoparticles.

ACKNOWLEDGMENTS

The authors thank to E. Aparicio-Ceja and I. Gradilla-Martínez for their technical helps in recording XRD and SEM images of the samples. The work was partially supported by CONACyT, Mexico (Grant No. 46269 and 47505).

[1] J. G. Lu, P. Chang, and Z. Fan, Mater. Sci. Eng., R. **52**, 49 (2006).
[2] H. De Waal and F. Simons, Thin Solid Films **77**, 253 (1981).
[3] J. G. Ekerdt, K. J. Klabunde, J. R. Shapley, J. M. White, and J. T. Yates, J. Phys. Chem. **92**, 6182 (1988).
[4] J. Watson, Sens. Actuators **5**, 29 (1984).
[5] N. S. Baik, G. Sakai, N. Miura, and N. Yamazoe, Sens. Actuators B **63**, 74 (2000).
[6] Y. He, J. C. Campbell, R. C. Murphy, M. F. Arendt, and J. S. Swinnea, J. Mater. Res. **8**, 3131 (1993).
[7] G. Li, X. Zhang, and S. Kaki, Sens. Actuators B **60**, 64 (1999).
[8] C. Kim, M. Noh, M. Choi, J. Cho, and B. Park, Chem. Mater. **17**, 3297 (2005).
[9] Z. W. Pan, Z. R. Dai, and Z. L. Wang, Science **291**, 1947 (2001).
[10] C. Guo, M. Cao, and C. Hu, Inorg. Chem. Commun. **7**, 929 (2004).
[11] G. Sakai, T. Nakatani, T. Yoshimura, M. Uota, and T. Kijima, Chem. Lett. **34**, 1364 (2005).
[12] J. Q. Hu, X. L. Ma, N. G. Shang, Z. Y. Xie, N. B. Wong, C. S. Lee, and S. T. Lee, J. Phys. Chem. B **106**, 3823 (2002).
[13] Y. Liu and M. Liu, Adv. Funct. Mater. **15**, 57 (2005).
[14] F. Paraguay-Delgado, W. Antúnez-Flores, M. Miki-Yoshida, A. Aguilar-Elguezabal, P. Santiago, R. Diaz, and J. A. Ascencio, Nanotechnology **16**, 688 (2005).
[15] L. Vayssieres and M. Graetzel, Angew. Chem., Int. Ed. **43**, 3666 (2004).
[16] JCPDS card No. 41-1445.
[17] D. Calestani, M. Zha, A. Zappettini, L. Lazzarini, G. Salviati, L. Zanotti, and G. Sberveglieri, Mater. Sci. Eng., C **25**, 625 (2005).
[18] G. Salviati, L. Lazzarini, M. Z. Zha, V. Grillo, and E. Carlino, Phys. Status Solidi A **202**, 2963 (2005).
[19] Q. Zhao, Y. Gao, X. Bai, C. Wu, and Y. Xie, Eur. J. Inorg. Chem. **2006**, 1643.
[20] T. W. Kim, D. U. Lee, J. H. Lee, D. C. Choo, M. Jung, and Y. S. Yoon, J. Appl. Phys. **90**, 175 (2001).
[21] X. L. Yuan, L. Lazzarini, G. Salviati, M. Zha, and T. Sekiguchi, Mater.

Sci. Semicond. Process. **9**, 331 (2006).
[22]G. Cheng, K. Wu, P. Zhao, Y. Cheng, X. He, and K. Huang, Nanotechnology **18**, 355604 (2007).
[23]H. He, Jr., T. H. Wu, C. L. Hsin, K. M. Li, L. J. Chen, Y. L. Chueh, L. J. Chou, and Z. L. Wang, Small **2**, 116 (2006).
[24]H. W. Kim, N. H. Kim, J. H. Myung, and S. H. Shim, Phys. Status Solidi A **202**, 1758 (2005).
[25]D. Maestre, A. Cremades, and J. Piqueras, J. Appl. Phys. **95**, 3027 (2004).
[26]S. S. Cheng and D. K. Park, Mater. Sci. Eng., B **95**, 55 (2002).
[27]J. M. Themlin, R. Sporken, J. Darville, R. Caudano, and J. M. Giles, Phys. Rev. B **42**, 11914 (1990).
[28]D. F. Crabtree, J. Phys. D **7**, L22 (1974).
[29]D. F. Crabtree, J. Phys. D **7**, L17 (1974).
[30]P. Y. Tu and M. Cardona, *Fundamentals of Semiconductors*, 2nd ed. (Spinger, Berlin, 1999), p. 448.
[31]J. X. Zhou, M. S. Zhang, J. M. Hong, and Z. Yin, Solid State Commun. **138**, 242 (2006).
[32]S. Fujihara, T. Maeda, H. Ohgi, E. Hosono, H. Imai, and S.-H. Kim, Langmuir **20**, 6476 (2004).
[33]J. Zhu, Z. Lu, S. T. Aruna, D. Aurbach, and A. Gedanken, Chem. Mater. **12**, 2557 (2000).
[34]K. Hsi, S. Kung, and K. F. Hayes, Langmuir **9**, 263 (1993).
[35]K. Dutta and S. K. De, Mater. Lett. **61**, 4967 (2007).
[36]K. Dutta and S. K. De, J. Phys. D **40**, 734 (2007).